On the Suitability of CubeSats in Earth Orbits for Radiation Testing of Interplanetary Payloads

Friederike Wolff [(1)(*)], Birgit Ritter[(2)], Stas Barabash[(2)]

[(1)] Luleå University of Technology, Rymdcampus 1, 98128 Kiruna, Sweden
[(2)] Institute of Space Physics, Rymdcampus 1, 98128 Kiruna, Sweden
[(*)] wolff.friederike@googlemail.com

ABSTRACT

One of the challenges faced when designing instruments for interplanetary missions is the radiation environment that will be encountered. The effects of this radiation are twofold: the total energy deposited by energetic particles in electronic components can result in transient or permanent damage. Energetic particles penetrating sensor heads result in background counts in detectors such as micro-channel plates or channel electron multipliers, thereby reducing the signal-to-noise ratio. Critical components, subsystems and whole instruments that are relatively small can be accommodated on CubeSats, flown in orbits around Earth and be tested there for their response to the terrestrial radiation belts. Although the fluxes and energies in low Earth orbit (LEO) are small on average, satellites in high-inclination orbits pass through the horns of the radiation belts, thereby being exposed mostly to relativistic electrons and protons. This paper gives an introduction to the radiation environment of typical low Earth orbits and elaborates on the suitability of CubeSats in such orbits as a test-bed for interplanetary missions. The goal of the J³ mission (Jupiter CubeSat) is presented as a case study: this CubeSat is designed to carry a micro-channel plate, a channel electron multiplier and a semiconductor detector and serves as a flight test for a detector subsystem for a particle instrument flying on ESA's Jupiter and Icy Moon Explorer (JUICE) mission. The radiation spectra in Earth orbit will be compared to those expected during the science phase of the JUICE mission.

1. Introduction

Ionizing particle radiation can have numerous effects on spacecraft and in particular its electronics from single event effects to permanent change of material properties through displacement damage. An issue that is of particular concern for missions that aim at the exploration of the Jovian environment is the presence of highly energetic electrons, which can penetrate spacecraft and instrument walls. In addition to the effects mentioned before, such electrons can induce false counts in instruments that contain particle detectors such as micro-channel plates (MCPs) or channel electron multipliers (CEMs), thereby decreasing the signal to noise ratio of the scientific measurements. Such detectors are often used in instruments that analyze plasma or other ions in the eV to keV range.

The subject of this study is a mission for technology demonstration and testing of a system to detect and discard measurements corrupted by penetrating radiation. An anti-coincidence shield based on a semiconductor will be used on the Jovian Plasma Dynamics and Composition Analyzer (JDC) on ESA's Jupiter and Icy Moon Explorer Mission (JUICE). Also, the response to penetrating radiation of MCPs and CEMs to be used on JUICE payloads shall be characterized. These systems make up the Radiation Test Experiment for JUICE (RATEX-J) payload shown in Figure 1, which shall be carried by J^3, a 1U CubeSat made up of only COTS components. The aim of this paper is the derivation of all science requirements for the J^3 mission as well as the prediction of scientific data that would be generated during such a mission.

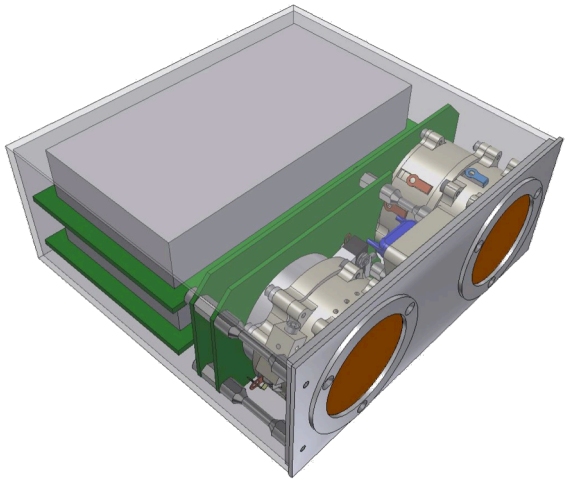

Figure 1 – RATEX-J instrument

1 Instrument Description

1.1 Particle Detectors

The RATEX-J instrument focuses on two kinds of particle detections commonly used in plasma instrumentation, namely MCPs (micro-channel plates) and CEMs (channel electron multipliers). Their principle of operation is the acceleration of incoming electrons by subjecting them to a large voltage across a channel which is shaped in such a manner that the electrons often collide with the walls as they pass through the detector, see Figure 3 and Figure 3. These surfaces also have a high secondary electron yield and through the resulting cascade gains of up to 10^8 for can be obtained.

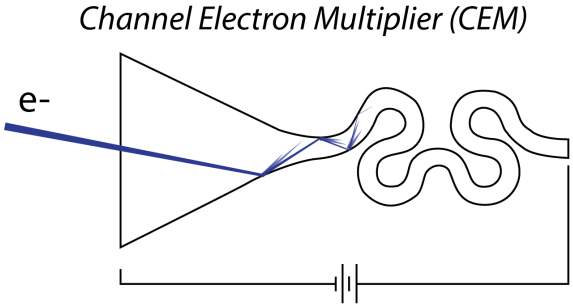

Figure 2 – Illustration of CEM operating principle

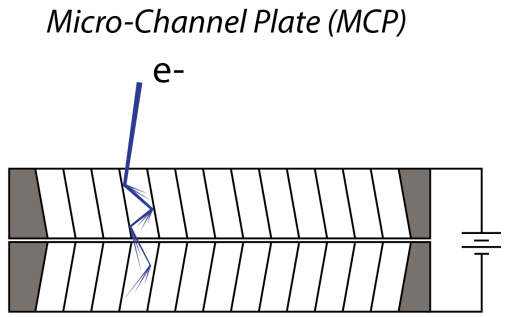

Figure 3 – Illustration MCP operating principle

1.2 Time-of-flight chambers

Both MCPs and CEMs will be used in a particle spectrometer to be flown on JUICE. In this instrument, a selection of ions depending on their energy-per-charge ratio is performed by an electrostatic analyzer. Subsequently, a time-of-flight chamber is used to determine the mass of the ions. The principle of the time-of-flight chamber illustrated in Figure 4: A beam of ions the mass of which shall be measured is directed at a start surface, from which it is reflected towards a stop surface. Those so-called conversion surfaces have the property of giving off electrons upon being impacted.

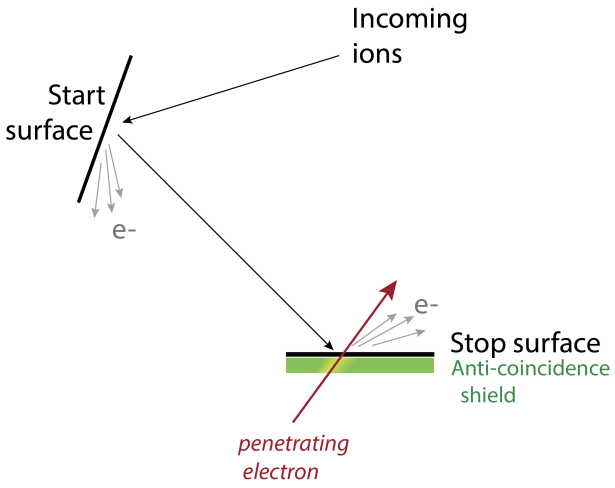

Figure 4 – Illustration of time-of-flight chamber with anti-coincidence system

These secondary electrons can be picked up by particle detectors (MCPs or CEMs) and used as start and stop signals to measure the time the ion took to travel through the chamber. The mass of the ion can then be obtained through the following formula:

$$m = \frac{2W}{(\frac{L}{t_1 - t_0})^2}$$

where m is the mass of the particle, t_1-t_0 is the time between the start and stop signal, W is the kinetic energy of the particle and L is the distance between the start and the stop surface.

1.3 Anti-coincidence system

The problem that arises when using such particle detectors in an environment with energetic electrons such as the Jovian magnetosphere is that such electrons can penetrate the instrument and produce false counts. One mitigation approach is the use of an anti-coincidence shield, which is also illustrated in Figure 2.

This system consists of a silicon detector, which is placed behind the stop surface. Such an arrangement will lead to the penetrating particle depositing energy in the silicon detector if it passes through a conversion surface. This way, false signals can be detected and discarded.

The RATEX-J payload contains two detector stacks one of which contains a MCP and the other a CEM. Both have a silicon detector to test the functionality of the anti-coincidence system.

2 Orbit Selection

The systems under test will ultimately be operated around Jupiter, therefore potential orbits are analysed for the similarity of their radiation environment to the Jovian one.
Since the satellite will be launched as a secondary payload, the orbits that were analysed were taken from the *Spaceflight Inc.* launch manifest [1]. All launch opportunities that are offered regularly (every year) have been investigated, namely three low-Earth orbits (LEO) two of which are sun-synchronous orbits (SSO). Two highly elliptical orbits (HEO) are offered one of which is a geostationary transfer orbit (GTO). The relevant orbital parameters are summarized in Table 2-1.

Table 2-1 - Description of orbits offered regularly by Spaceflight, retrieved March 2015

	Orbit type	Altitude [km]	Inclination [°]
1	SSO	700 (range: 600-830)	98.2
2	SSO	500	97.4
3	HEO	15000 x 39000	63.4
4	GTO	185 x 36000	27
5	LEO	550 (range: 500-600)	63.4

The fluxes encountered in those orbits have been obtained using SPENVIS (Space Environment Information System) [2]. The averaged data is shown in Figure 5. The accuracy of the electron model used here (AE-8) is often quantified by stating a factor of two for its uncertainty [3]. However, a recent evaluation of data from the Van Allen probes has concluded that for LEO, the fluxes given by AE-8 often overestimate the very complex and highly variable electron environment (up to two orders of magnitude for the energy range between 2 and 3 MeV) [4].
Given this difficulty on predicting even the order of magnitude of the electron fluxes, if can be said that the difference between the different LEO orbits is very small and within the range of available altitudes. The highly elliptical orbits would offer a two order of magnitude increase in flux. For various reasons it is not possible to develop a CubeSat for such an orbit using only COTS systems, but such launch opportunities could be used for radiation testing missions in the future.

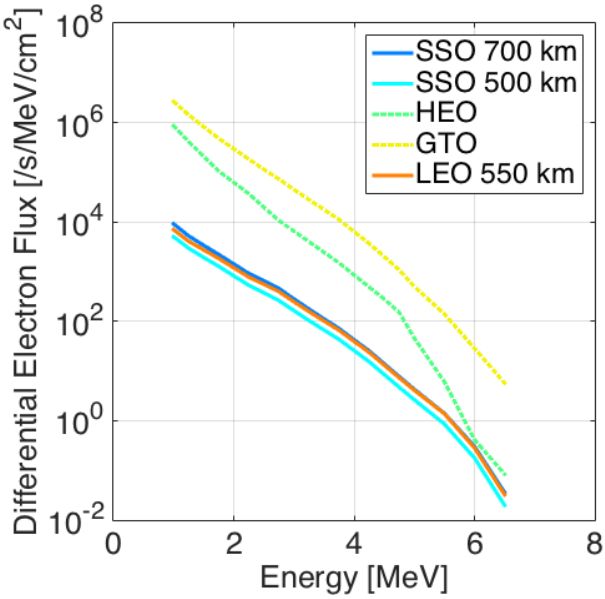

Figure 5 – Average electron fluxes corresponding to orbits of regularly offered launch opportunities

Figure 6 shows how the flux varies over a typical high inclination LEO orbit. The highest fluxes occur at approximately 60° latitude when the satellite traverses the horns of the radiation belts. The SAA (South Atlantic Anomaly) is also clearly visible.

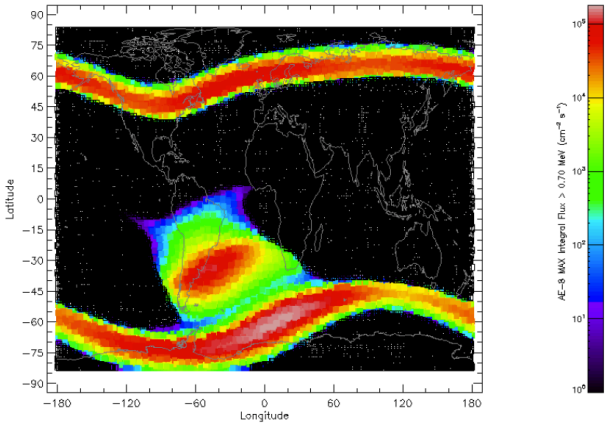

Figure 6 – Flux map of a 700 km Sun-Synchronous Orbit

Figure 7 compares the average electron flux of a LEO orbit to the environment expected during JUICE [5]. The cut-off energy for in LEO is approximately 6 MeV while the Jovian environment contains electrons in the 10 MeV range in significant numbers and even extends into the GeV range. It can be seen that the average fluxes in LEO are at least one order of magnitude smaller than those predicted for JUICE.

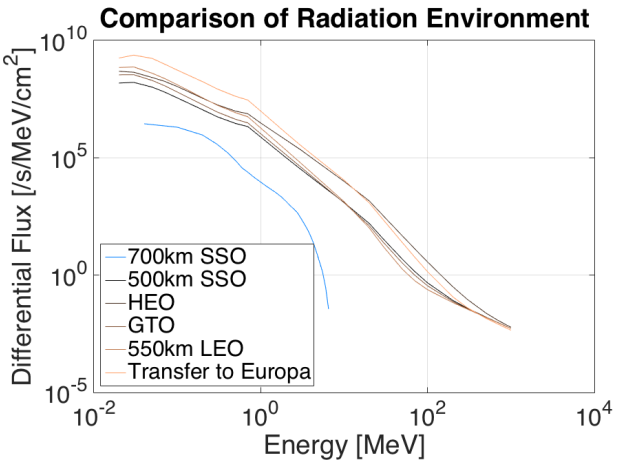

Figure 7 – Average Earth fluxes compared with fluxes predicted for JUICE

Figure 8 shows the instantaneous fluxes in a LEO orbit at the southern radiation belt crossing and in the south Atlantic anomaly. In the SAA, the flux in the Earth-bound orbit matches the lowest flux phase of JUICE up to energies of 300 keV. Beyond that, the Earth-bound fluxes are at least one order of magnitude lower than the Jovian fluxes. Although the low energy fluxes are significantly higher in the SAA, the radiation belt crossings have higher fluxes at higher energies as well as a higher cut-off energy. It will be shown later that only electrons with energies of more than approximately 1.5 MeV can penetrate through the sensor stack. Because the radiation belt crossings have higher fluxes of energetic electrons, those regions are of primary interest for this mission.

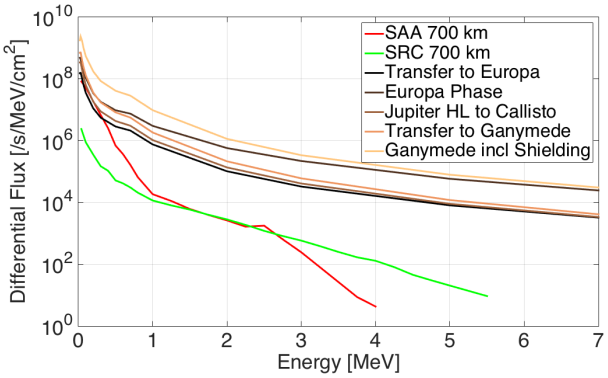

Figure 8 – Maximum LEO Earth fluxes compared with fluxes predicted for JUICE

In order to pass through the horns of the radiation belts, the most important orbital parameter is the inclination, which must be at least 63°. Furthermore, it has been found that an inclination close to this value yields a higher average flux as the satellite spends more time in the high-flux zones as opposed to a polar satellite. The orbital altitude only has a negligible effect within the feasible range for CubeSats (< 800 km). The lowest altitude that was analysed was 500 km. Lower altitudes were not investigated because the current launch opportunities do not include orbits of both lower altitude and high inclination.

3 Operational Requirements

Figure 9 shows the fraction of time the satellite spends in high-flux zones for different energies and orbits. A “high” flux for a given energy is defined as 0.01 times the maximum flux at this energy in a 700 km SSO. It can be seen that a duty cycle of approximately 20% must be accounted for.

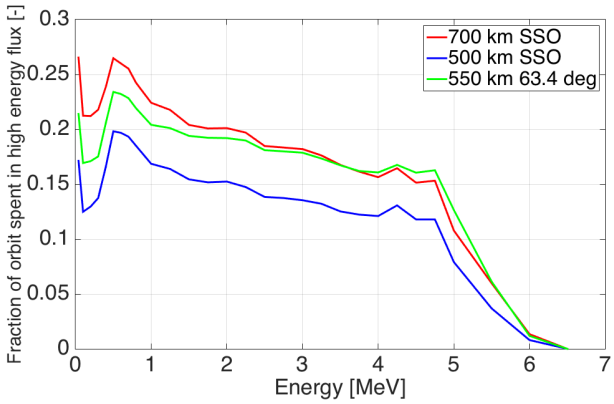

Figure 9 – Fraction of time spent in high-flux zones

Figure 10 displays how the flux varies over one orbit. The corresponding ground track is depicted in Figure 11. It should be noted that although the radiation belt crossing are traversed four times every orbit, a pass through the SAA only occurs on some orbits and the duration of this additional high-flux interval is strongly dependent on the longitude of the ascending node.

The satellite must therefore not only be able to operate the instrument at a duty cycle of at least 20%, but also do so in the high-flux zones which occur at latitudes around ±60°.

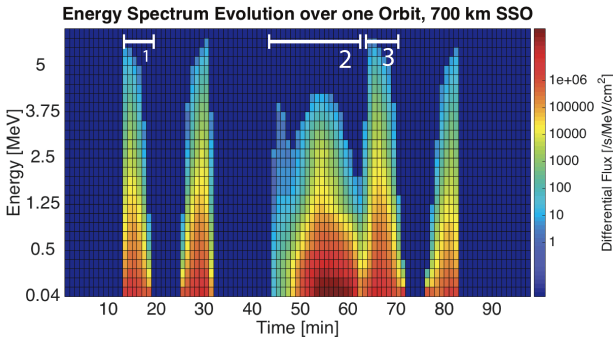

Figure 10 – Variation of flux over one orbit (1: northern radiation belt crossing, 2: SAA, 3: southern radiation belt crossing)

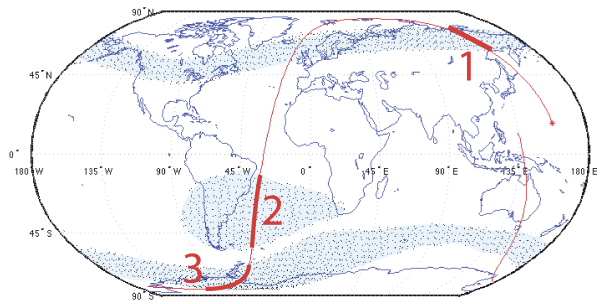

Figure 11 – Ground track corresponding to Figure 10

4 Flux directivity

The electron flux is strongly directional due to the manner in which the magnetosphere influences the electron motion. The most important effects are the following:

Bounce motion: Trapped electrons perform an adiabatic bounce motion between the magnetic poles. Over this motion energy is conserved, but exchanged between the components parallel and perpendicular to the field. When the motion parallel to the field is reduced to zero, the electron reverses direction. This point is called the mirror point.

Gyration: Charged particles that are subjected to a magnetic field perform a circular motion around the field line. The radius of this motion is determined by the magnetic field strength and velocity component perpendicular to the field line.

Although another component of electron motion is the drift around the Earth, this occurs on timescales that are much longer compared to the other effects listed here [6]. Therefore, this effect has be neglected for the following analysis.

Pitch angle variation: As a consequence of the bounce motion, the angle between the electron velocity and the field changes with field strength. The angle increases as the electron moves closer to the poles until it reaches 90° at the mirror point. An illustration of this variation is shown in Figure 12.

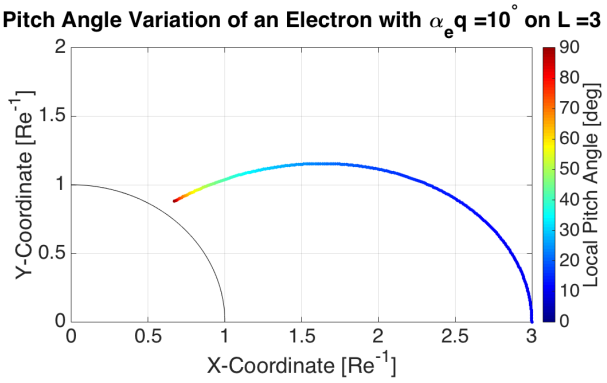

Figure 12 – Pitch angle variation from the equator to the mirror location close to the pole

No data exists on the directivity of the electron flux close to the poles, but data from the Van Allen probes is available on the directivity of the fluxes on the magnetic equator [4]. The pitch angle distributions from the magnetic equator have been mapped to those at the locations of interest using a simple dipole model for the

Earths magnetic field. The details of this analysis can be found in [7]. Figure 13 illustrates the angular distribution of flux. The flux is highest at angles of 60° with respect to the magnetic field line and drops to almost zero in the direction perpendicular to it.

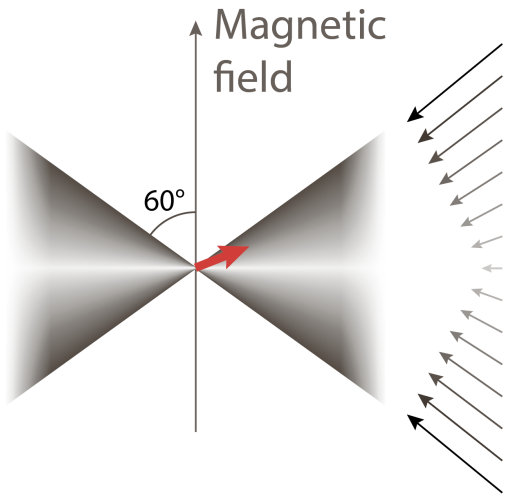

Figure 13 - Illustration of flux directivity in the radiation belt crossings: The magnetic field points in the vertical direction. The detector viewing direction is indicated by the red arrow. The darker the shading in the direction of pointing, the higher the flux from this direction. The same is indicated by the length of the arrows. The angular distribution of flux is axially symmetric around the magnetic field vector.

5 Simulation of Instrument Response

In order to determine the instrument response, the GRAS (Geant4 Radiation Analysis for Space) tool was used [8]. This software is based on Geant4 [9], which is a toolkit to simulate the passage of particles through matter using Monte-Carlo simulation. GRAS allows the user to easily set up typical space radiation analyses, e.g. total ionizing dose (TID) or non-ionizing energy loss (NIEL). The setup is then simulated with Geant4.

The instrument geometry in the simulation consists of cylinders of different thicknesses corresponding to the relevant parts of the detector stack and is shown in Figure 14. The outer surface of the detector stack which faces the space environment is a titanium foil and will in the following be referred to as the top of the detector stack. Below, the silicon detector is located which is mounted on an alumina substrate. The aluminium foil takes the role of the stop surface on this arrangement and acts as a nominal electron source.

The output of a simulation with a 2 MeV electron beam source is visualized in Figure 15.

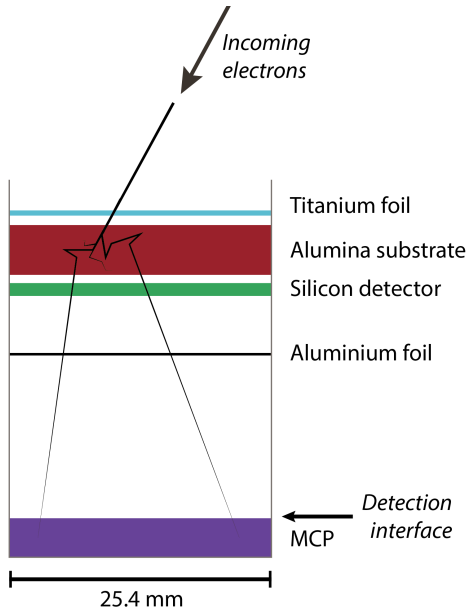

Figure 14 – Model of detector stack used in the Simulations. The sketch is not to scale.

The way in which particles are created in GRAS is through the specification of a General Particle Source (GPS). This source can be assigned specifications such as shape and angle under which particles are to be generated, but it is not flexible enough to generate a radiation environment with the characteristics described previously. Therefore, the following approach has been used:

The omnidirectional flux from SPENVIS is used to determine the number of particles that impact on the outer surface of the detector stack. This quantity is called the experienced flux. Using the previously presented pitch angle distributions, a probability density function was derived which quantifies the probability of an electron being at a certain angle relative to the field line. This function has been called directional flux density. A second function, called the throughput function, was defined as the number of particles arriving at the MCP per incoming electron of a certain angle. This function was found through simulation.

The product of the experienced flux, the directional flux density and the throughput function was integrated over entire hemisphere that corresponds to the instrument field of view, yielding the count rate on the MCP. The details of this calculation can be found in the [7].

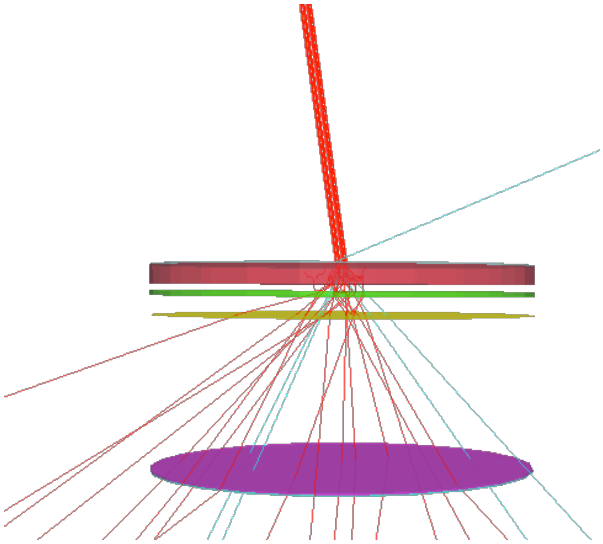

Figure 15 – Simulation of the interaction of a particle beam with the detector stack. Red and cyan tracks represent electrons and gammas, respectively. The source energy is 2 MeV.

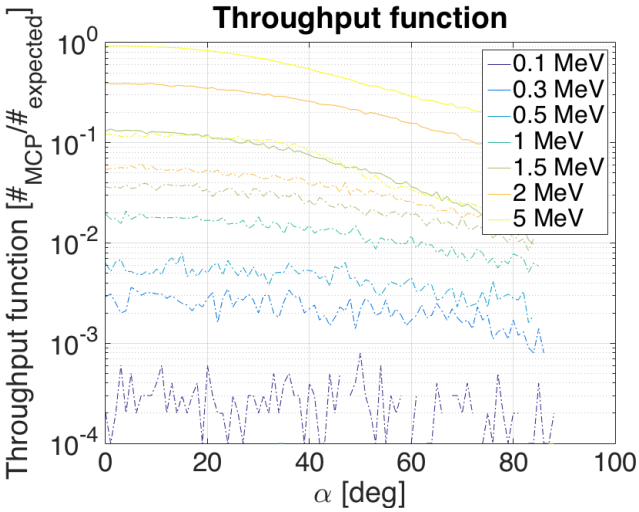

Figure 16 – Fraction of particles arriving on the MCP per unit of particles impacting the top of the detector stack (dash-dot: gammas, solid line: electrons)

Figure 16 shows the number of particles detected on the MCP per unit of electrons that enter the detector stack and its variation with angle between the particle's initial direction and the instrument viewing direction. Since the particle detectors are sensitive to both electrons and gamma radiation, the throughput functions for both are shown.

It can be seen that electrons below approximately 1.5 MeV cannot penetrate the sensor stack. Instead, they loose energy in the upper layers of the stack, thereby generating gamma radiation. Although the electrons loose all their energy before reaching the bottom and do not directly result on a count on the MCP, the gammas that they generate travel through the stack in an undisturbed manner and are registered on the MCP.
The higher energy electrons result in an electron flux on the MCP that is one order of magnitude higher than the gamma flux provided that the source is mono-energetic.
In general, the registered gamma counts show less dependence on the angle of the incoming particles.

6 Expected count rates and spectra of Flux on detector

Figure 17 shows the fraction of particles impacting the detector stack for the spectrum encountered in the southern radiation belt crossing (SRC). It can be seen that the fractions of electrons and gammas that are received on the MCP are of the same order of magnitude. This is explained by the large fluxes of low-energy electrons in the input spectrum, which generate few gammas per electron, but add up to a number comparable to that of the electrons generated by the smaller flux of higher energy.

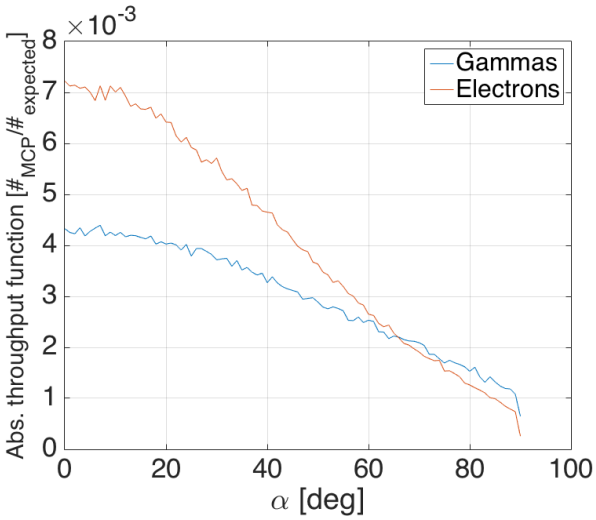

Figure 17 – Total number of particles on MCP per particle impacting the detector stack as a function of angle of incident particle

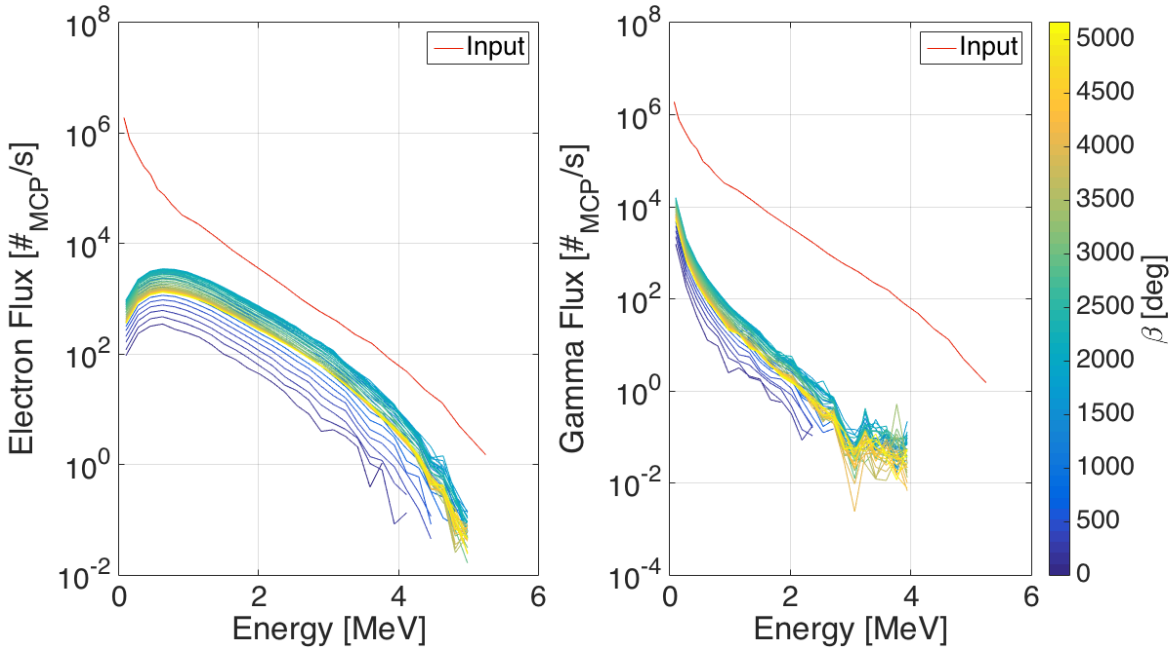

Figure 18 – Predicted electron and gamma spectra on the MCP for the southern radiation belt crossing as a function of instrument orientation. β is the angle between the instrument viewing direction and the magnetic field line

Figure 18 show the electron and gamma spectra on the MCP as a function of the angle between the instrument viewing direction and the magnetic field line (β). The red line gives the electron input spectrum for reference. The electron flux on the MCP peaks at 0.5 MeV whereas the gamma flux increases sharply towards the low end of the spectrum. Figure 19 shows the same dataset for the electron spectra as a function of β and it can be seen that the maximum count rate occurs when the instrument is at an angle of 33° with the magnetic field line.

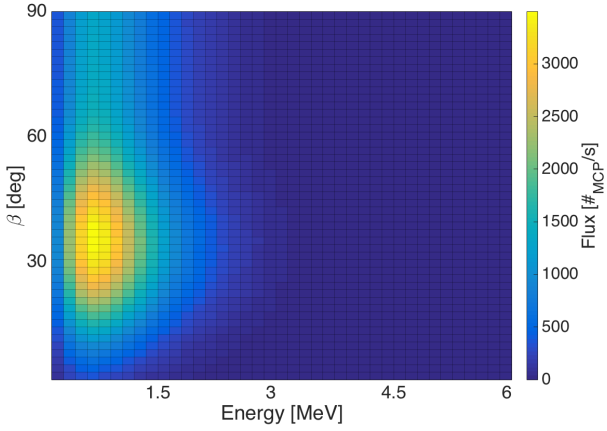

Figure 19 – Predicted electron spectra in the southern radiation belt crossing

Figure 20 shows the predicted count rate as a function β. The count rate peaks at 33° and falls to almost zero when the detector is aligned with the field line (β=0°). When increasing the angle beyond 33°, the count rate falls but approaches a constant value of less then half the maximum above a β-angle of 65°. From this Figure, an attitude control accuracy of ±15° has been deduced.

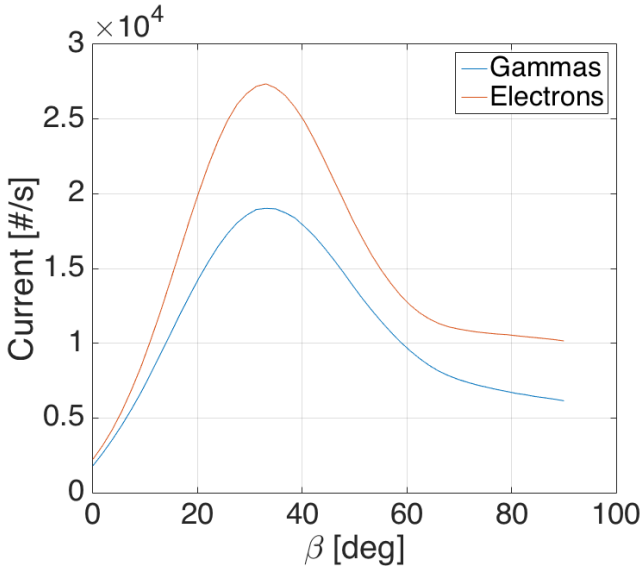

Figure 20 – Count rate on MCP in the southern radiation belt crossing

7 Summary

The science requirements have been derived by investigating the average electron fluxes for different orbits that are typical for CubeSats as well as from the variation of the fluxes within these orbits. The directivity of these fluxes has been derived and the detector response to the predicted radiation environment has been simulated. Based on this analysis, the following science requirements have been formulated:

- The orbital inclination must be greater than 63°.

- The bus must be able to operate the instrument throughout every radiation belt crossing.
  This corresponds to four operation periods per orbit and is equivalent to a duty cycle of at least 20%.

- During operation, the angle between the instrument vector and the magnetic field line shall be 33° or 147° and shall be kept with an accuracy of ±15°.

The predicted count rates in the radiation belt crossings are in the order of 10^4 per second.

8 References

[1] *Spaceflight Inc. Launch Schedule*, http://spaceflightservices.com/manifest-schedule/

[2] *Space Environment Information System, (SPENVIS),* https://www.spenvis.oma.be/

[3] *AP8MIN and AP8MAX Trapped Proton Models*. https://creme.isde.vanderbilt.edu/CREME-MC/help/ap8min-and-ap8max-trapped-proton-models, January 2015.

[4] X. Li. *Upper Limit on the Inner Radiation Belt MeV Electron Intensity*. Journal of Geophysical Research: Space Physics, 120, 2014.

[5] T.-E. . SRE-PAP. *JUICE Environmental Specification. Technical report*, European Space Research and Technology Centre, 2014.

[6] M. Walt. *Introduction to Geomagnetically Trapped Radiation*. Cambridge University Press, Cambridge, 1994.

[7] F. Wolff. *J3 and its Radiation Environment, V4*. IRF Kiruna, Sweden, 2015.

[8] *GRAS – Geant4 Radiation Analysis for Space,* http://space-env.esa.int/index.php/geant4-radiation-analysis-for-space.html

[9] *Geant4*, http://geant4.cern.ch/